

# Effect of Platform Dimension on the Dendrite Growth and Stray Grain Formation in a Ni-Base Single-Crystal Superalloy

X.B. MENG, J.G. LI, Z.Q. CHEN, Y.H. WANG, S.Z. ZHU, X.F. BAI, F. WANG, J. ZHANG, T. JIN, X.F. SUN, and Z.Q. HU

A model of typical turbine blade shape with different platforms was designed to study the nucleation and growth of stray grains in the platforms by both experimental investigation and a ProCAST simulation based on a cellular automaton finite-element model. The results show that at the withdrawal rate of 5 mm/min, no stray grains nucleate in the small dimensional platform. However, the primary grain grows into the inner and outer sections of this platform in different manners due to different thermal conditions in these sections. Furthermore, with the increase of platform dimension, stray grains with random orientations gradually nucleate in the corners of the platforms. It is found that these stray grains tend to nucleate either in the inner corners or at a faster withdrawal rate, which is associated with the corresponding thermal condition. Based on these results, the rule of the critical platform dimension and withdrawal rate without stray grain formation has been proposed. Besides, the simulation results are in accordance with experimental findings.

DOI: 10.1007/s11661-012-1527-4

© The Minerals, Metals & Materials Society and ASM International 2012

## I. INTRODUCTION

IN the past decades, Ni-base superalloy single-crystal turbine blades have been extensively used in the modern gas turbine for aircraft propulsion and power generation. Compared with conventionally casting blades, they can be subjected to higher service temperature and possess superior mechanical properties due to the elimination of grain boundary (GB). However, owing to the complex geometry shape of turbine blades and the increased addition of refractory alloy content, the prevention of defect formation in modern turbine blades during the directional solidification (DS) process becomes increasingly challenging.

One of the major defects encountered during the DS process is stray grain,<sup>[1-4]</sup> which is randomly oriented and easily forms high-angle boundaries (HABs) with primary grain. Since GB strengthening elements are absent in single crystal, HABs are very harmful for the mechanical properties and usually perform as the source for crack initiation. Therefore, many investigations<sup>[1-24]</sup> have

been carried out to study the behavior of dendrite growth and the formation of stray grains. The platform of turbine blade, which is considered as the most sensitive site where stray grains tend to nucleate, has already been paid fully attention to. Napolitano and Schaefer<sup>[5]</sup> investigated the growth of dendrites and the formation of low-angle GBs in the platform. Newell and Souza *et al.*<sup>[9,10]</sup> thought the cumulative misorientation of low-angle GB in the platform results from plastic deformation of dendrite stems in response to contraction stresses during the DS process. Yang *et al.*<sup>[14]</sup> simulated the formation of stray grains in the platform by cellular automaton finite-difference model and found that increasing either the withdrawal rate or the inclination angle of isotherm is in favor of the nucleation and growth of stray grains. Ma *et al.*<sup>[24]</sup> simulated the thermal condition in the platform of turbine blades and proposed that the heat conductor technology could reduce stray grain formation in the platform.

However, few studies are aimed at the effect of platform dimension on the formation of stray grains. Therefore, some studies should be performed in this field. In this article, it is concerned with the effect of platform dimension on the dendrite growth and stray grain formation. To reach this goal, a model of typical turbine blade shape with different platforms is designed. The behavior of dendrite growth and the formation of stray grains in these platforms are investigated by both experimental investigation and numerical simulation. Besides, the effect of withdrawal rate on the formation of stray grains in the platforms is also discussed. It is expected to deeply understand the reasons why stray grains nucleate and grow in these platforms, and the relationship among stray grain

---

X.B. MENG, Assistant Professor, J.G. LI, T. JIN, and X.F. SUN, Professors, and Z.Q. HU, Academician, are with the Institute of Metal Research, Chinese Academy of Sciences, Shenyang 110016, P.R. China. Contact e-mail: xbmeng@imr.ac.cn Z.Q. CHEN, Y.H. WANG, S.Z. ZHU, and X.F. BAI, Engineers, are with the Aviation Industry Corporation of China (AVIC) Shenyang Liming Aero-engine (Group) Corporation LTD., Shenyang 110043, P.R. China. F. WANG, Engineer, is with the Aviation Industry Corporation of China (AVIC) Guiyang Liyang Aero-engine (Group) Corporation LTD., Guiyang 550002, P.R. China. J. ZHANG, Professor, is with the State Key Laboratory of Solidification Processing, Northwestern Polytechnical University, Xi'an 710072, P.R. China.

Manuscript submitted June 11, 2011.

Article published online December 1, 2012

formation, platform dimension, and withdrawal rate will be revealed.

## II. EXPERIMENTS

To investigate the effect of platform dimension on the formation of stray grains, both experiment and simulation have been conducted based on a model of typical turbine blade shape.

### A. Experimental Details

#### 1. Model design

A model of typical turbine blade shape with one body and four different platforms (1, 2, 3, and 4 marked in Figure 1(b)) was designed to investigate the effect of platform dimension on the formation of stray grains, as shown in Figure 1. Several parameters used in this model are labeled in Figure 1, including the length (L), the width (W), the height (H), and the position of platform (P). The details of the geometrical dimension and distribution position of body and platforms are shown in Table I.

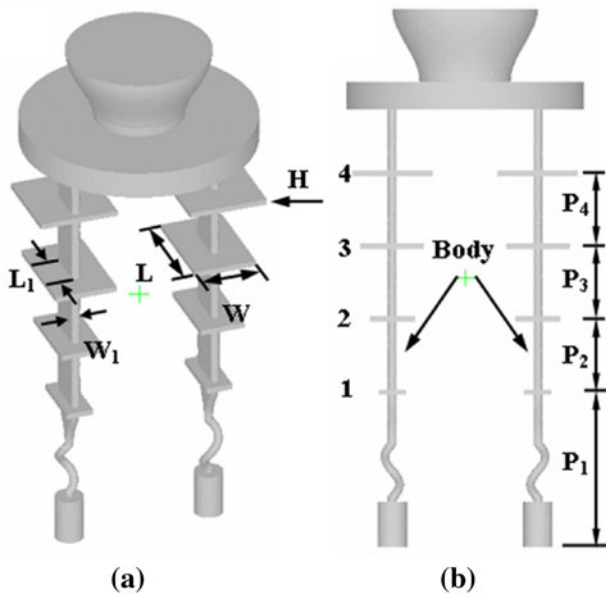


Fig. 1—Schematic diagram of the parameters in the model design.

Table I. Geometrical Dimensions of Platforms Design in this Study

No.	Geometry	Dimension (L × W × H)/mm <sup>3</sup>	Position (mm)
1	Cuboid (S)	25 × 5 × 160	Body
2	Cuboid (S)	35 × 15 × 3	$P_1 = 90$
3	Cuboid (S)	45 × 25 × 3	$P_1 + P_2 = 130$
4	Cuboid (S)	55 × 35 × 3	$P_1 + P_2 + P_3 = 170$
5	Cuboid (A)	48(32 + 16) × 44 × 3	$P_1 + P_2 + P_3 + P_4 = 210$

S: symmetric; A: asymmetric.

#### 2. Procedure of experiments

The DS experiment was carried out in a Bridgman (high-rate solidification) industrial vacuum furnace. The alloy used in current study is a typical second-generation Ni-base superalloy CMSX-4 with the nominal composition (wt pct) of 6.4Cr, 9.6Co, 0.6Mo, 6.4W, 6.6Ta, 2.9Re, 5.7Al, 1.0Ti, 0.1Hf, and rest Ni. After induction melting in the crucible, the master alloy was poured into a ceramic mold mounted on a water-cooled copper chill plate in the center of the furnace chamber. After about 600 s heat preservation for thermal equilibrium, the mold was withdrawn at the rate of 5 mm/min.

The as-cast grain structures in the platforms were observed by an optical microscope to investigate the dendrite growth and stray grain formation. The nucleation and growth of stray grains were investigated by electron backscatter diffraction (EBSD) technology in an S-3400N scanning electron microscope (Hitachi Ltd., Tokyo, Japan), equipped with Channel 5 software (Oxford instruments, Oxford, UK) for automatic grain indexing and mapping.

Ni-single crystal was used to calibrate precision of crystallographic measurements. Grain orientations were specified with respect to a coordinate system based on the sample geometry, and the Z axis in this coordinate system was parallel to the direction of dendrite growth. Since the diffracted electrons that produce the patterns for indexing can only escape from the top 10 to 20 nm of the surface, a highly polished, deformation-free, flat surface is required in order to collect high-quality EBSD data. The sample surface was machined by wire electrodischarge machining to acquire a flat plane perpendicular to the direction of dendrite growth. An accelerating voltage of 20 kV and a beam current of 5 nA were employed to collect EBSD patterns by both area-scan and linear-scan modes with steps of 20 μm and 50 μm, over several zones multiplied by 50 times on every sample. More details could be referred to the corporate standard of Q/KJ 08.01-4-2010.

#### B. Simulation Details

The ProCAST software (ESI Group, Paris, France) based on a cellular automaton finite-element (CAFE) model was used for the simulation. Thermal condition and the fluid flow during the DS process were calculated by a macroscale ProCAST model with a finite-element solution of energy and momentum equations, and then the calculated thermal profiles were input into the microscale CAFE model to predict grain structures and orientation evolutions.<sup>[25–29]</sup>

### III. RESULTS AND DISCUSSION

#### A. Experiment

##### 1. Dendrite growth and stray grain formation

Grain structures in different platforms of the model with typical turbine blade shape are shown in Figure 2. In the macrostructure of the designed model in Figure 2(a), no stray grains nucleate are observed in platform 1, whereas many stray grains are present in platforms 2, 3, and 4. In the dendrite structure of Figure 2(b), it can be seen that the primary grain grows into platform 1 completely, and no stray grains nucleate in this platform. However, as shown in Figures 2(c) through (e), with the increase of platform dimension, stray grains increasingly nucleate in the corners of the platforms, grow toward the center in the form of dendrites, block the growth of primary grain, and restrict the primary grain in the center of the platform.

##### 2. Dendrite growth in platform 1

In platform 1, the primary grain grows into this platform by developing new higher order dendrites, but these higher order dendrites of primary grain grows in the inner section and outer section of this platform in different manners. In this work, the inner section is toward the center and the outer section is toward the furnace wall.

Figure 3 shows the evolution of dendritic structure and accumulated misorientation in the inner section of platform 1. As shown in Figure 3(a), in the inner section, the primary grain develops secondary dendrites to grow into the platform laterally, and then these secondary dendrites develop tertiary dendrites parallel to the growth direction of primary grain to occupy the platform. In Figures 3(b) and (d), the results show the dendrites continuously rotate, and the accumulated

misorientation of dendrites fluctuates up and down. The rotation of dendrite tips probably results from the solidification contraction of the melting which could induce the residual stress and plastic deformation in the tips of dendrites.<sup>[9,10]</sup> Furthermore, as shown in Figures 3(c) and (d), the area scan results show that no obvious subgrain boundary appears in the inner section of platform 1.

However, in the outer section, the dendritic structure is complex. Figure 4 shows the evolution of the dendritic structure and the accumulated misorientation in the outer section of platform 1. Secondary dendrites grow laterally into the outer section and develop tertiary dendrites parallel to the primary grain. Since the outer section is close to the furnace, the thermal condition changes from heat soak to heat extraction quickly when the mold is withdrawn from the heating zone to the vacuum chamber. It is easy to reach a larger thermal gradient at the edge of outer section. Therefore, the secondary dendrites could develop tertiary dendrites earlier at the edge of outer section, and these tertiary dendrites at the edge grow much faster than the tertiary dendrites close to the center. When the tertiary dendrites grow upward at the edge, they develop higher order dendrites again. The higher order dendrites at the edge grow toward the center of platform and meet the tertiary dendrites near the center. Finally, a complex dendritic structure in the outer section is obtained, as indicated by white arrows in Figures 4(a).

In Figures 4(b) and (d), the EBSD results show that the misorientation of dendrites also fluctuates up and down. As shown in Figures 4(c) and (d), the area scan results show that a subgrain boundary forms. Based on these results, it is implied that the orientation of high-order dendrite tips at the edge is misoriented with the orientation of high-order dendrite tips near the center,

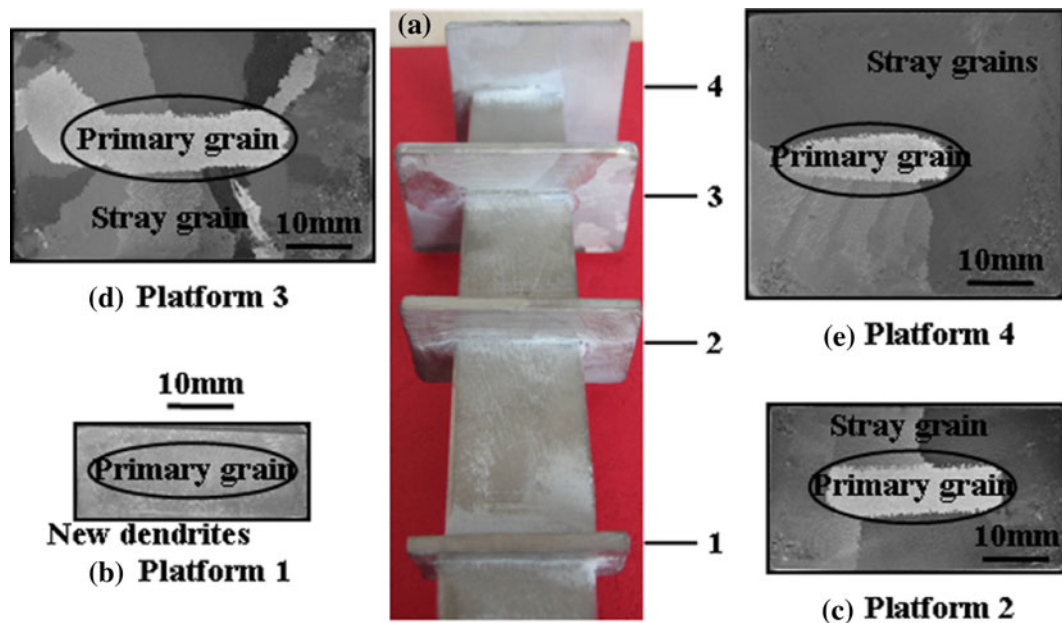
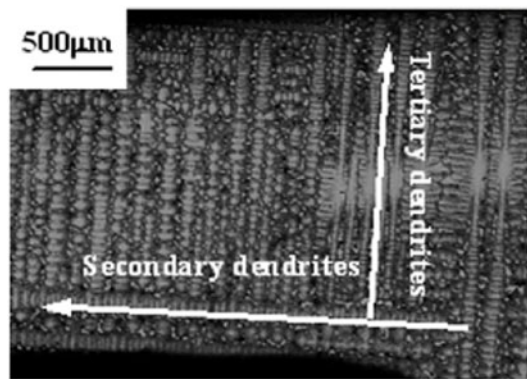
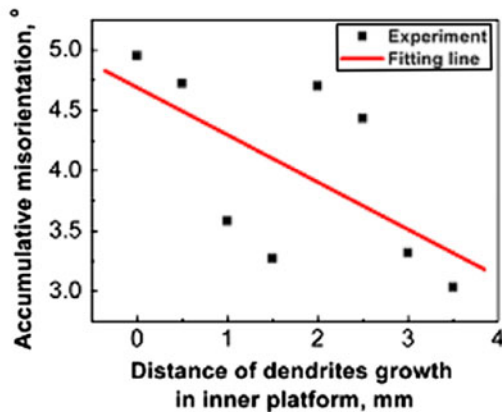


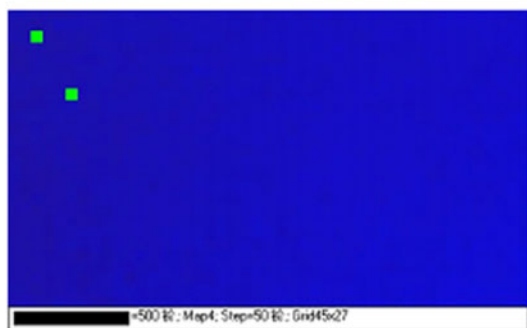
Fig. 2—Grain structure in the platforms of the model: (a) macrostructure of models with different platforms and microstructure of the cross section in platforms (b) 1, (c) 2, (d) 3, and (e) 4.



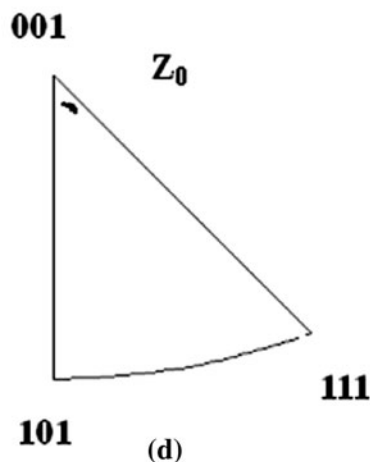
(a)



(b)



(c)



(d)

Fig. 3—Evolution of dendritic structure and accumulated misorientation in the inner section of platform 1: (a) behavior of dendrite growth (indicated by arrows), (b) accumulated misorientation, (c) orientation evolution by area scan, and (d) corresponding inverse pole figures.

and this misorientation varies with the growth of dendrites. Therefore, a subgrain boundary forms when the high-order dendrites with different growth directions meet each other again.

### 3. Nucleation and growth of stray grains

With the increase of the platform dimension, stray grains increasingly nucleate in the corners of the platforms and grow toward the center in the form of dendrites. The nucleation and growth of stray grains in platform 2 is investigated to show the process of stray grain formation.

The microstructures of stray grains in different positions of platform 2 are shown in Figure 5. In Figures 5(a) and (b), many small stray grains nucleate in the corners and grow toward the center of the platform in the form of dendrites. They compete with each other, and only several stray grains can survive. Figures 5(c) and (d) show the GB between primary grain and stray grain near the center of platform 2. The higher order dendrites of the primary grain meet stray grain and stop growing near the center of platform 2.

Figure 6 shows the grain structures and the corresponding inverse pole figures in different positions of

platform 2. Figure 6(a) shows that the orientations of stray grains are random when they nucleate in the corners of platform 2. It is implied that many stray grains with random orientation have nucleated in the corners of platform 2 before the high-order dendrites developed by the primary grain reach there. As shown in Figure 6(b), only one stray grain (B) reaches the center, and the primary grain (A) meets this stray grain near the center. It is suggested that after nucleation, stray grains compete with each other and only few of them survive. They grow toward the center in the form of dendrites, and meet the primary grain near the center. As a result, the primary grain (A) is blocked in the center by stray grains and could not grow into platform 2. Therefore, at the perimeter of the primary grain in platform 2, HABs form (Figure 6(b)).

The nucleation and growth of stray grains in platforms 3 and 4 are similar to that in platform 2. However, with the increase of platform dimension, the amount and size of stray grains increase sharply.

### 4. Nucleation tendency of stray grains in the platforms

Stray grains are easy to nucleate in the corners of the platforms and grow into the platforms in the form of

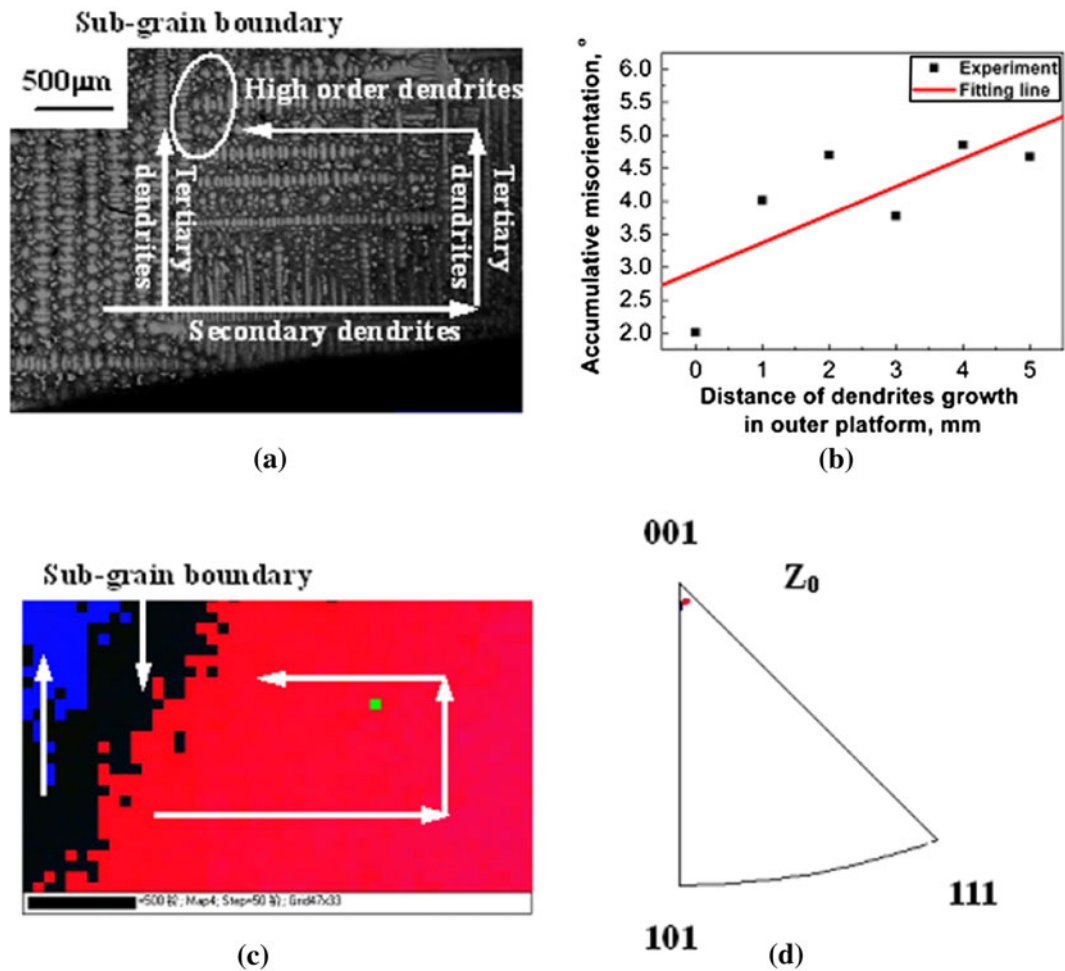


Fig. 4—Evolution of dendritic structure and accumulated misorientation in the outer section of platform 1: (a) behavior of dendrite growth (indicated by arrows), (b) accumulated misorientation, (c) orientation evolution by area scan, and (d) corresponding inverse pole figures.

dendrites. To clearly reveal the effect of corners positions on the nucleation of stray grains, the corners of platforms are divided into two groups: two inner corners and two outer corners. Figure 7 shows the number of platform corners where stray grains nucleate. As shown in this figure, no stray grains nucleate in the corners of platform 1. But in platform 2, stray grains nucleate in two corners, both of which are inner corners. Furthermore, in platforms 3 and 4, stray grains nucleate in three corners, including two inner corners and one outer corner.

These results indicate that with the increase of the platform dimension, stray grains are much easier to nucleate in the platform corners. The reason is that with the increase of platform dimension, the melting in the corners of the platform could reach a larger undercooling; therefore, stray grains are easier to nucleate in the corners of larger dimensional platforms. Besides, based on these results, it is also concluded that the nucleation tendency of stray grains is different in the corners of the platforms. As shown in Figure 7, stray grains tend to nucleate in the inner corners. In platforms 2, 3, and 4, stray grains nucleate in each inner corner. In contrast,

stray grains nucleate in no outer corner of platform 2 and only one outer corner of platforms 3 and 4.

## B. Simulation

### 1. Thermal condition

The accuracy of thermal condition has an important influence on the simulation. Experimentally measured temperature/time boundary conditions and a second-generation single-crystal superalloy CMSX-4 with temperature-dependent physical properties were used in this study. The temperature of the heating zones and the vacuum withdrawal chamber were 1873 K (1600  $^{\circ}\text{C}$ ) and 293 K (20  $^{\circ}\text{C}$ ), respectively. The alloy was poured at 1773 K (1500  $^{\circ}\text{C}$ ) into the mold with the same temperature (1773 K [1500  $^{\circ}\text{C}$ ]). After heat preservation for 600 seconds, which aims to reach thermal equilibrium in the mold, the castings were withdrawn at different rates of 1, 3, 5, 6, and 12 mm/min. More details about the simulation parameters during the DS process have been reported previously.<sup>[26–28]</sup> The calculated thermal condition at the rate of 5 mm/min when the liquidus isotherm reaches platform 1 at 1700 seconds is shown in Fig-

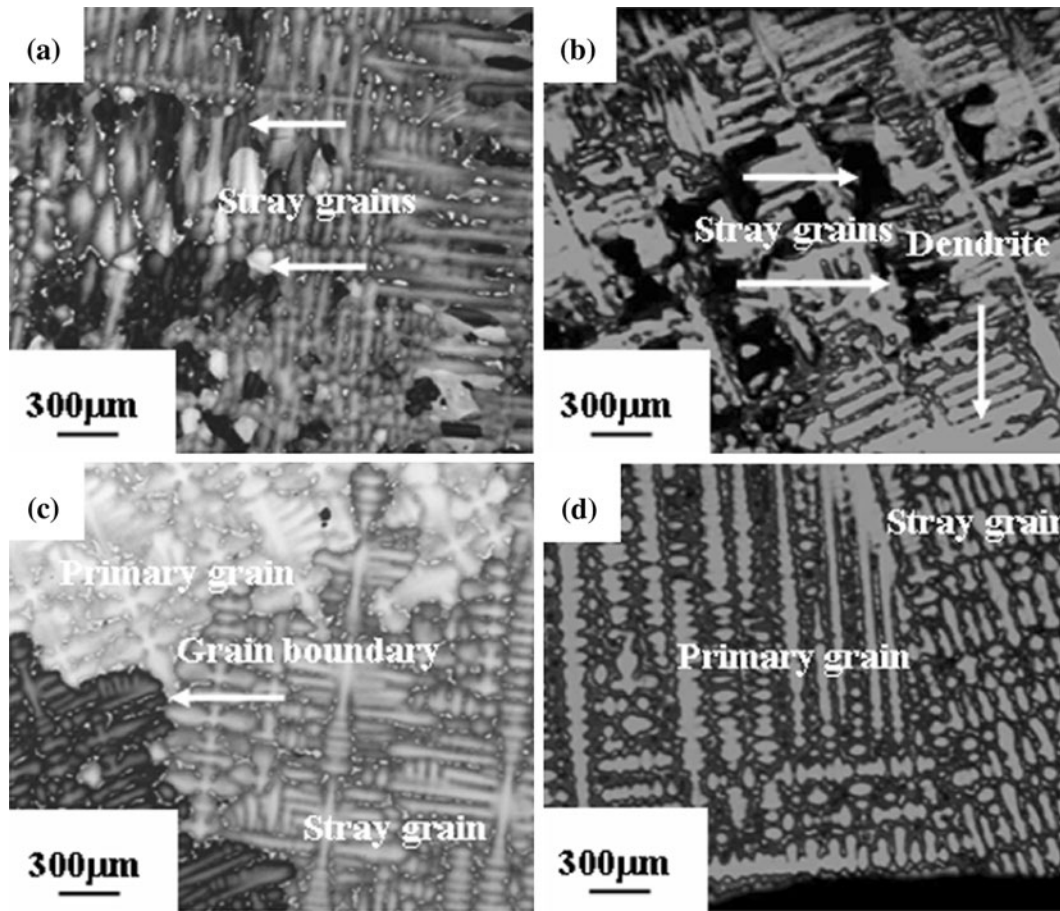


Fig. 5—Microstructure of the cross section and the vertical section in platform 2: (a), (b) nucleation of stray grains in the corners; (c), (d) GB between primary grain and stray grain near the center.

ure 8(a). An enlarged view of the thermal conditions and the thermal condition of cross section in this platform are shown in Figures 8(b) and (c). The calculated thermal condition reveals the solidification sequence (Figure 8(b)) and the liquidus isotherm shape (Figure 8(c)) in platform 1, which is very useful for the analysis of grain growth and stray grain formation in this platform.

### 2. Dendrite growth and stray grain formation in platforms

The calculated thermal conditions were then used as inputs to predict grain structures using a CAFE model. The surface nucleation density of  $10^8/\text{m}^2$ <sup>[26,27]</sup> was applied in this study.

The predicted grain structures of the model and the cross sections of the platforms with different dimensions at the rate of 5 mm/min are shown in Figure 9. In this work, different colors represent different oriented grains. Figure 9(a) generally shows the grain structures in the four different platforms. It can be seen that the amount and size of stray grains increases rapidly with the dimension of the platforms increasing. Figures 9(b) through (e) show the grain structures on the cross section of the different platforms. In Figure 9(b), the primary grain grows into platform 1 completely, and no stray grains nucleate in this platform. With the increase of the

platform dimension (Figures 9(c) through (e)), stray grains increasingly nucleate in the corners of the platforms and grow toward the center; however, the primary grain could not grow into these platforms and the occupation space of the primary grain decreases sharply. Besides, these simulation results agree well with the experiments.

### 3. Thermal condition in platform 1

Compared with the inner section, the dendritic structure is complex in the outer section of platform 1. To understand the reason why dendrites grow in different manners in this platform, the thermal conditions at the rate of 5 mm/min in both the inner section and the outer section were calculated at the time when the temperature of the corresponding positions reached the liquidus temperature.

In Figures 10(a1) and (a2), it is shown that the liquidus isothermal becomes radial when the temperature of platform 1 approaches to the liquidus temperature. Furthermore, compared with the inner section, the outer section has a larger thermal gradient, which implies the secondary dendrites grow faster in the outer section than that in the inner section (Figures 10(b1), (b2), (c1), and (c2)). The reason is the outer section is close to the furnace, and the thermal condition changes

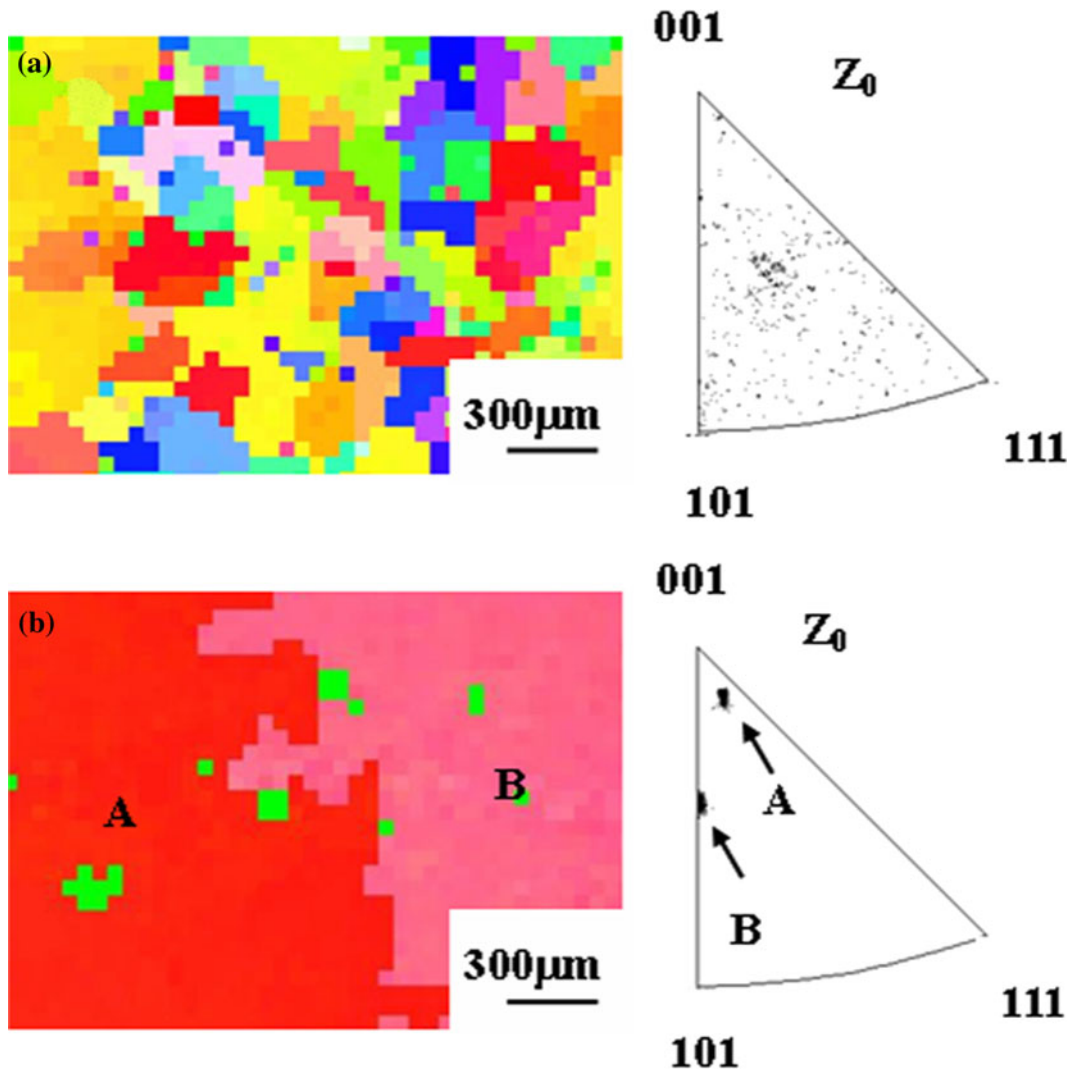


Fig. 6—Grain structures and corresponding inverse pole figures in platform 2: (a) nucleation of stray grains in the corners and (b) GB between stray grain and primary grain in the center.

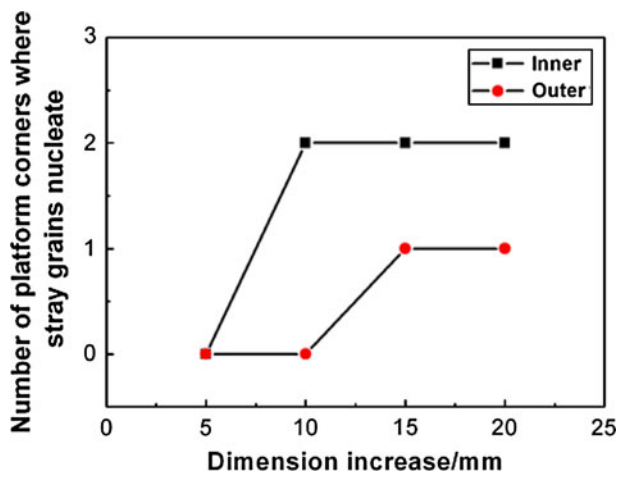


Fig. 7—Number of platform corners where stray grains nucleate.

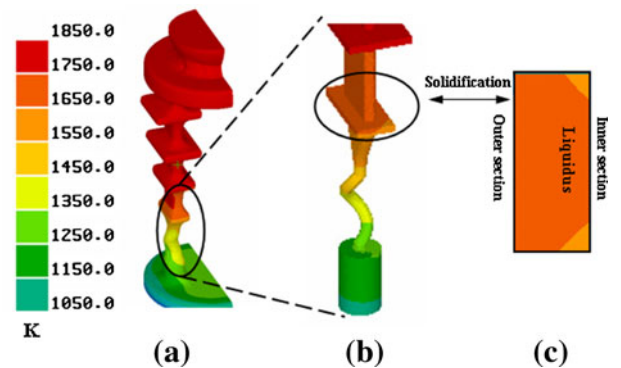


Fig. 8—Predicted thermal condition at 1700 s when the liquidus isotherm reaches platform 1: (a) the mold, (b) enlarged view of platform 1, and (c) the cross section of the first platform.

from heat soak to heat extraction rapidly when the mold is withdrawn from the heating zone to the vacuum chamber. However, the heat exchange in the inner section from heat soak to heat extraction is blocked off by the body and the outer section during the DS process. Therefore, compared with the inner section, it is easy to

reach a larger axial (Figures 10(b1) and (b2)) and longitudinal (Figures 10(c1) and (c2)) thermal gradient at the edge of the outer section. In this work, the axial direction is from the inner side to the outer side, and the longitudinal direction is the direction of directional solidification. This larger axial thermal gradient causes the secondary dendrites grow faster in the outer section, especially at the edge of the outer section. The larger longitudinal thermal gradient induces the secondary dendrites develop tertiary dendrites at the edge of the outer section. As a result, a complex dendritic structure is obtained in the outer section.

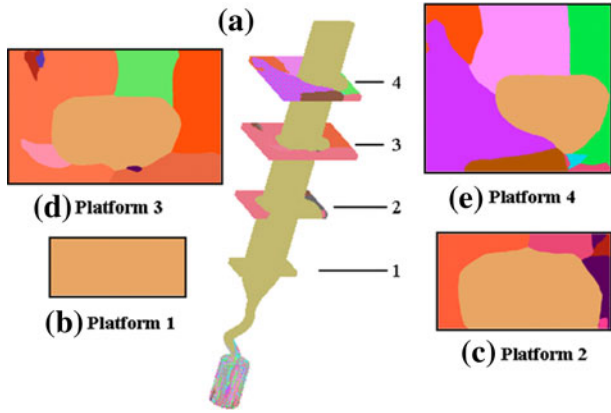


Fig. 9—Predicted grain structures of the model (a) and the cross sections of platform (b) 1, (c) 2, (d) 3, and (e) 4.

#### 4. Nucleation of stray grains in different positions of platforms

The formation of stray grains in different positions of the platforms is related to the evolution of thermal condition. To reveal the reason why different nucleation tendency of stray grains is present in the different corners of platform 2, the evolution of the thermal conditions at the rate of 5 mm/min on the cross section and the vertical section were calculated when the liquidus reached this platform. As shown in Figures 11(a1) and (a2), the temperature of the inner corners first reaches the liquidus temperature, which

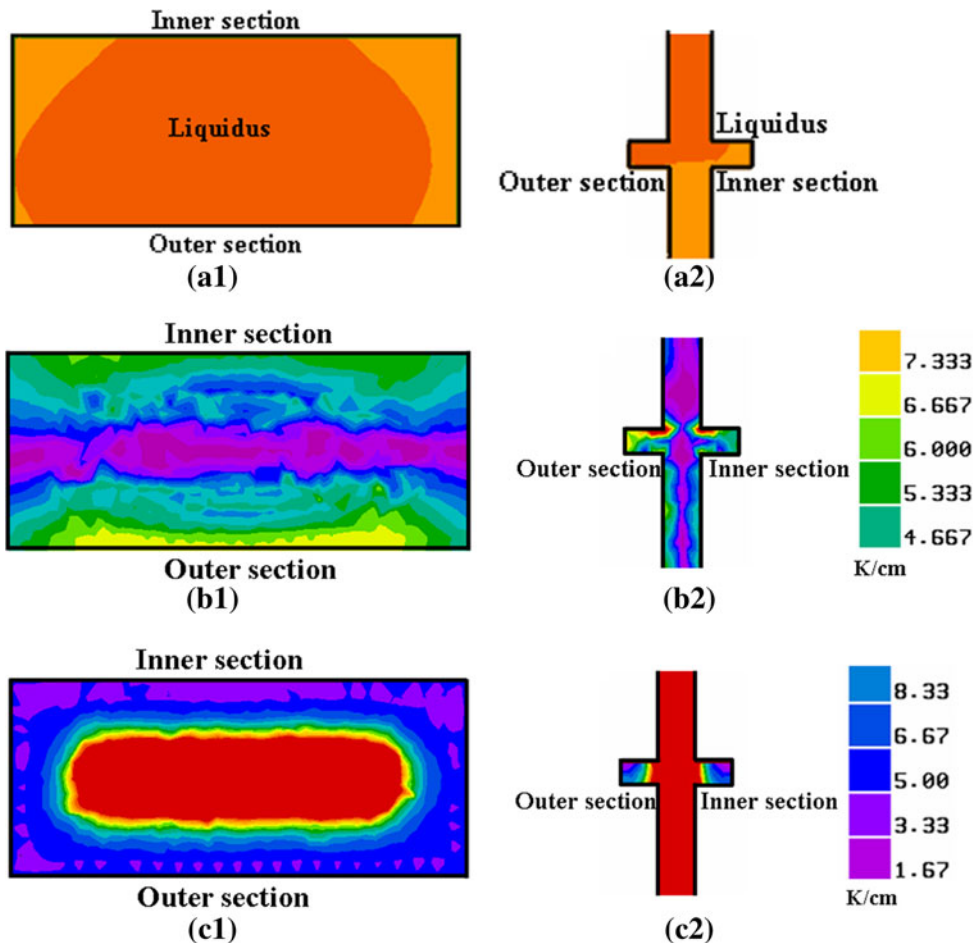


Fig. 10—Liquidus isothermal, axial, and longitude thermal gradient when the temperature of corresponding positions reached the liquidus temperature in platform 1.



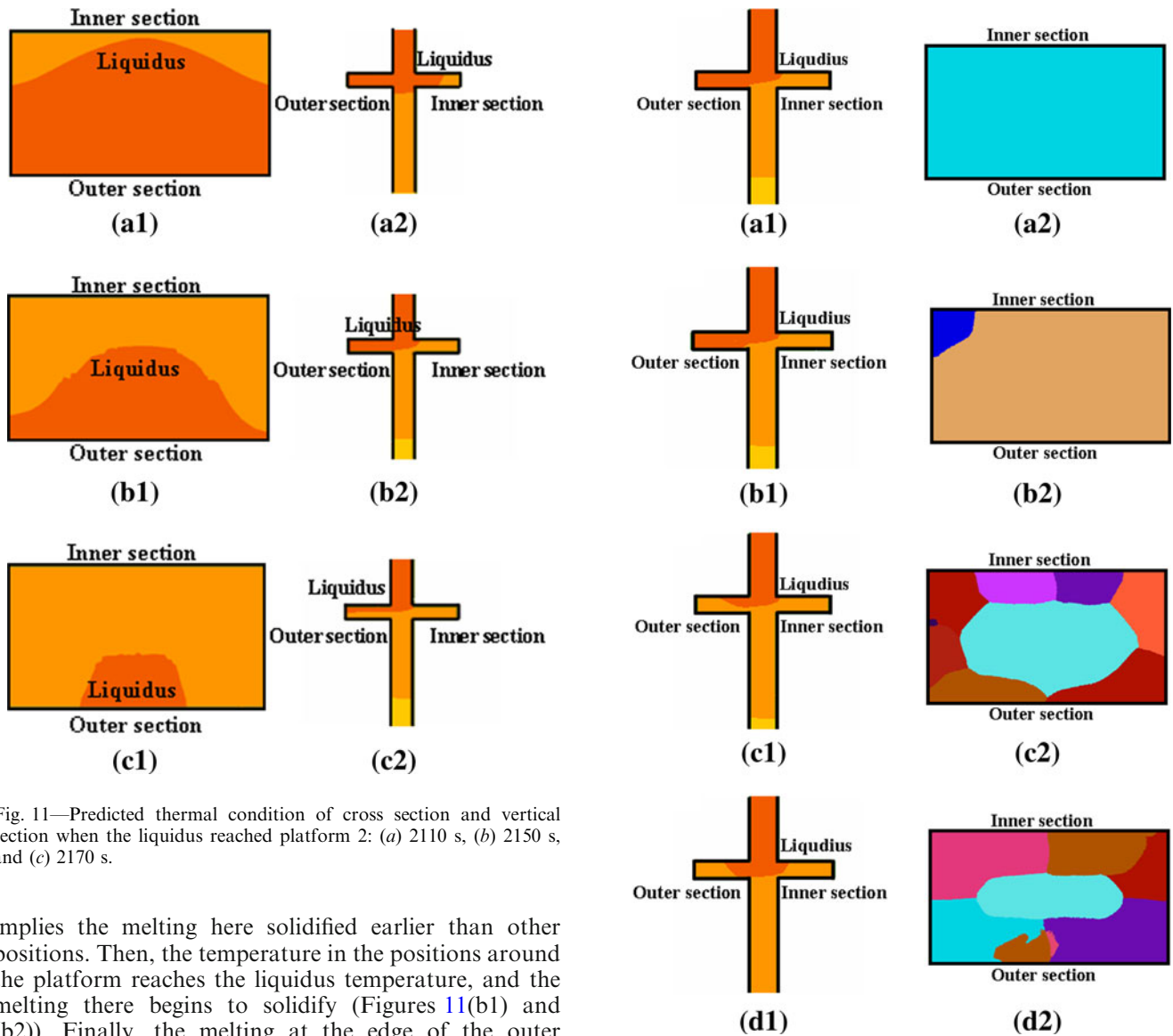


Fig. 11—Predicted thermal condition of cross section and vertical section when the liquidus reached platform 2: (a) 2110 s, (b) 2150 s, and (c) 2170 s.

implies the melting here solidified earlier than other positions. Then, the temperature in the positions around the platform reaches the liquidus temperature, and the melting there begins to solidify (Figures 11(b1) and (b2)). Finally, the melting at the edge of the outer section solidifies (Figures 11(c1) and (c2)). Based on these simulation results, it is shown that when the liquidus isothermal approaches to the platform, the curvature of the solidification front gradually became concave, and the melting in the corners of the inner section begins to solidify first (Figures 11(a1) and (a2)). Therefore, stray grains are easier to nucleate first in the inner section of the platforms.

##### 5. Effect of withdrawal rate on the formation of stray grains

The withdrawal rate plays a significant role in the evolution of thermal condition and the formation of stray grains. The predicted thermal condition and grain structures in platform 2 at different withdrawal rates of 1, 3, 6, and 12 mm/min are simulated to investigate the effect of withdrawal rate on the formation of stray grains. At the withdrawal rate of 1 mm/min, when the liquidus isothermal approaches to platform 2, the curvature of the solidification front becomes inclined (Figure 12(a1)) and the primary grain grows into this platform completely (Figure 12(a2)). However, with the

Fig. 12—Predicted thermal condition and grain structures in platform 2 at different withdrawal rates of (a) 1, (b) 3, (c) 6, and (d) 12 mm/min.

increase of withdrawal rate, liquidus isothermal is gradually concave (Figures 12(b1) through (d1)) and stray grains with random orientation increasingly nucleate in platform 2 (Figures 12(b2) through (d2)). Besides, it is implied that with the withdrawal rate increasing, the amount and size of stray grains increases obviously, and the occupation space of the primary grain decreases sharply. Therefore, with the withdrawal rate increasing, stray grains tend to nucleate and grow in the platforms.

##### C. Rule of Platform Without Stray Grain Formation

Based on the results presented above, the rule of the critical platform dimension and withdrawal rate without stray grain formation has been proposed here. As shown in Figure 13, stray grains tend to nucleate in the corners of these platforms with the increase of platform dimension

## ACKNOWLEDGMENTS

This work was accomplished by the help of Dr. J.J. Liang and Dr. H. Meng, and it was financially supported by the National Basic Research Program (973 Program) of China under grant 2010CB631200 (2010CB631206), the National Natural Science Foundation of China (NSFC) under grants 51204156, 50931004, 50971124, 50904059, and 51071165; and the fund of the State Key Laboratory of Solidification Processing in NWPU under grant SKLSP201112. The authors are grateful for that support.

## REFERENCES

1. T.M. Pollock, W.H. Murphy, E.H. Goldman, D.L. Uram, and J.S. Tu: *Superalloys 1992*, S.D. Antolokch, R.W. Stusrud, R.A. MacKay, D.L. Anton, T. Khan, R.D. Kissinger, and D.L. Klarstrom, eds., TMS, Warrendale, PA, 1992, pp. 125–34.
2. M. Meyer ter Vehn, D. Dedecke, U. Paul, and P.R. Sahn: *Superalloys 1996*, R.D. Kissinger, D.J. Deye, D.L. Anton, A.D. Cetel, M.V. Nathal, T.M. Pollock, and D.A. Woodford, eds., TMS, Warrendale, PA, 1996, pp. 471–79.
3. M.C. Schneider, J.P. Gu, C. Beckermann, W.J. Boettinger, and U.R. Kattner: *Metall. Mater. Trans. A*, 1997, vol. 28A, pp. 1517–31.
4. J.P. Gu, C. Beckermann, and A.F. Giamei: *Metall. Mater. Trans. A*, 1997, vol. 28A, pp. 1533–42.
5. R.E. Napolitano and R.J. Schaefer: *J. Mater. Sci.*, 2000, vol. 35, pp. 1641–59.
6. S. Tin and T.M. Pollock: *J. Mater. Sci.*, 2004, vol. 39, pp. 7199–205.
7. D. Goldschmidt, U. Paul, P.R. Sahn, D. Goldschmidt, U. Paul, and P.R. Sahn: *Superalloys 1992*, S.D. Antolokch, R.W. Stusrud, R.A. MacKay, D.L. Anton, T. Khan, R.D. Kissinger, and D.L. Klarstrom, eds., TMS, Warrendale, PA, 1992, pp. 155–64.
8. A. de Bussac and C.A. Gandin: *Mater. Sci. Eng. A*, 1997, vol. 237, pp. 35–42.
9. M. Newell, K. Devendra, P.A. Jennings, and N. D'Souza: *Mater. Sci. Eng. A*, 2005, vol. 412, pp. 307–15.
10. N. D'Souza, M. Newell, K. Devendra, P.A. Jennings, M.G. Ardakani, and B.A. Shollock: *Mater. Sci. Eng. A*, 2005, vols. 413–414, pp. 567–70.
11. Q.Y. Xu, B.C. Liu, Z.J. Liang, J.R. Li, S.Z. Liu, and H.L. Yuan: *Mater. Sci. Forum*, 2006, vol. 508, pp. 111–16.
12. J. Yu, Q.Y. Xu, B.C. Liu, J.R. Li, and H.L. Yuan: *Adv. Mater. Res.*, 2007, vols. 26–28, pp. 947–51.
13. W. Wang, A. Kermanpur, P.D. Lee, and M. McLean: *J. Mater. Sci.*, 2003, vol. 38, pp. 4385–91.
14. X.L. Yang, H.B. Dong, W. Wang, and P.D. Lee: *Mater. Sci. Eng. A*, 2004, vol. 386, pp. 129–39.
15. M. Rappaz, C.A. Gandin, J.L. Desbiolles, and Ph. Thevoz: *Metall. Mater. Trans. A*, 1996, vol. 27A, pp. 695–705.
16. R. Schadt, I. Wagner, J. Preuhs, and P.R. Sahn: *Superalloys 2000*, T.M. Pollock, R.D. Kissinger, R.R. Bowman, K.K. Green, M. McLean, S.L. Olson, J.J. Schirra, eds., TMS, Warrendale, PA, 2000, pp. 211–18.
17. P. Auburtin, T. Wang, S.L. Cockcroft, and A. Mitchell: *Metall. Mater. Trans. B*, 2000, vol. 31B, pp. 801–11.
18. P. Auburtin, S.L. Cockcroft, A. Mitchell, and T. Wang: *Superalloys 2000*, T.M. Pollock, R.D. Kissinger, R.R. Bowman, K.K. Green, M. McLean, S.L. Olson, and J.J. Schirra, eds., TMS, Warrendale, PA, 2000, pp. 255–61.
19. W.H. Yang, W. Chen, K.M. Chang, S. Mannan, and J. de Barbadillo: *Metall. Mater. Trans. A*, 2001, vol. 32A, pp. 397–406.
20. Y.Z. Zhou: *Scripta Mater.*, 2011, vol. 65, pp. 281–84.
21. W.J. Boettinger, S.R. Coriell, A.L. Greer, A. Karma, W. Kurz, M. Rappaz, and R. Trivedi: *Acta Mater.*, 2000, vol. 48, pp. 43–70.
22. J.D. Hunt and S.Z. Lu: *Metall. Mater. Trans. A*, 1996, vol. 27A, pp. 611–23.
23. A. Kermanpur, N. Varahram, P. Davami, and M. Rappaz: *Metall. Mater. Trans. B*, 2000, vol. 31B, pp. 1293–1304.

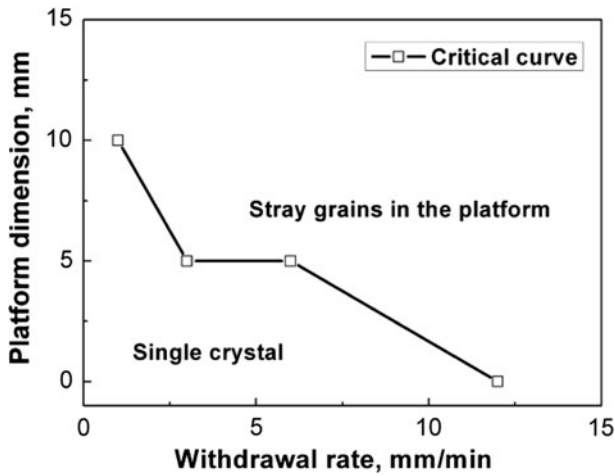


Fig. 13—Calculated critical platform dimension and withdrawal rate without stray grain formation.

and withdrawal rate. When the withdrawal rate is 1 mm/min, no stray grains are observed in platform 2 but many stray grains nucleate in platform 3. However, when the withdrawal rates are increased to 3 or 6 mm/min, many stray grains have already nucleated in platform 2. When the withdrawal rate is sequentially increased to 12 mm/min, stray grains are present in platform 1. Therefore, the critical platform dimension and withdrawal rate without stray grain formation in the platform are given in this figure, which is very helpful for the production of single-crystal turbine blade without stray grain formation in the platform.

## IV. CONCLUSIONS

The effect of platform dimension on the dendrite growth and stray grain formation was studied by both experiment and simulation. According to the results, following conclusions can be drawn:

1. Primary grain grows into the small dimensional platform by developing new high-order dendrites. However, primary grain grows in this small platform in different manners due to different thermal conditions in the inner and outer sections.
2. With the increase of the platform dimension, stray grains with random orientations increasingly nucleate in the corners of the platform, especially in the inner corners. They compete with each other, grow toward the center in the form of dendrites, and meet higher order dendrites of the primary grain to form HABs.
3. The nucleation tendency of stray grains is different. Stray grains nucleate easily in the inner corners, which is associated with the solidification sequence and the withdrawal rate in the platforms.
4. The withdrawal rate plays a significant role in the formation of stray grains. With the increase of withdrawal rate, stray grains tend to nucleate and grow in the platforms.
5. The simulation results agree well with experimental findings.

24. D.X. Ma and A. Bührig-Polaczck: *Metall. Mater. Trans. B*, 2009, vol. 40B, pp. 738–48.
25. H.J. Dai, J.C. Gebelin, M. Newell, R.C. Reed, N. D'Souza, P.D. Brown, and H.B. Dong: *Superalloys 2008*, R.C. Reed, K.A. Green, P. Caron, T.P. Gabb, M.G. Fahrman, E.S. Huron, and S.A. Woodard, eds., TMS, Warrendale, PA, 2008, pp. 367–74.
26. X.B. Meng, J.G. Li, T. Jin, X.F. Sun, C.B. Sun, and Z.Q. Hu: *J. Mater. Sci. Technol*, 2011, vol. 27 (2), pp. 118–26.
27. X.B. Meng, Q. Lu, J.G. Li, T. Jin, X.F. Sun, J. Zhang, Z.Q. Chen, Y.H. Wang, and Z.Q. Hu: *J. Mater. Sci. Technol*, 2012, vol. 28 (3), pp. 214–20.
28. X.B. Meng, Q. Lu, X.L. Zhang, J.G. Li, Z.Q. Chen, Y.H. Wang, Y.Z. Zhou, T. Jin, X.F. Sun, and Z.Q. Hu: *Acta Mater.*, 2012, vol. 60, pp. 3965–75.
29. P. Carter, D.C. Cox, C.A. Gandin, and R.C. Reed: *Mater. Sci. Eng. A*, 2000, vol. 280, pp. 233–46.